NeuroImage: Clinical 39 (2023) 103493

Contents lists available at ScienceDirect

NeuroImage: Clinical

journal homepage: www.elsevier.com/locate/ynicl

Mixed longitudinal and cross-sectional analyses of deep gray matter and white matter using diffusion weighted images in premanifest and manifest Huntington's disease

Beini Hu [a], Laurent Younes [b], Xuan Bu [c], Chin-Fu Liu [a], J. Tilak Ratnanather [a], Jane Paulsen [d,e], Nellie Georgiou-Karistianis [f], Michael I. Miller [a], Christopher Ross [g], Andreia V. Faria [c,*]

[a] Department of Biomedical Engineering, Johns Hopkins University, Baltimore, MD, USA
[b] Department of Applied Mathematics and Statistics, Johns Hopkins University, Baltimore, MD, USA
[c] Department of Radiology, School of Medicine, Johns Hopkins University, Baltimore, MD, USA
[d] Department of Psychiatry, Neurology, Psychological Brain Sciences, University of Iowa, USA
[e] Department Neurology, University of Wisconsin-Madison, USA
[f] School of Psychological Sciences and Turner Institute of Brain and Mental Health, Monash University, Australia
[g] Department of Psychiatry, School of Medicine, Johns Hopkins University, Baltimore, MD, USA

A R T I C L E I N F O

Keywords:
DTI
MRI
Huntington's disease
Longitudinal
Cross-sectional

A B S T R A C T

Changes in the brain of patients with Huntington's disease (HD) begin years before clinical onset, so it remains critical to identify biomarkers to track these early changes. Metrics derived from tensor modeling of diffusion-weighted MRIs (DTI), that indicate the microscopic brain structure, can add important information to regional volumetric measurements. This study uses two large-scale longitudinal, multicenter datasets, PREDICT-HD and IMAGE-HD, to trace changes in DTI of HD participants with a broad range of CAP scores (a product of CAG repeat expansion and age), including those with pre-manifest disease (i.e., prior to clinical onset). Utilizing a fully automated data-driven approach to study the whole brain divided in regions of interest, we traced changes in DTI metrics (diffusivity and fractional anisotropy) versus CAP scores, using sigmoidal and linear regression models. We identified points of inflection in the sigmoidal regression using change-point analysis. The deep gray matter showed more evident and earlier changes in DTI metrics over CAP scores, compared to the deep white matter. In the deep white matter, these changes were more evident and occurred earlier in superior and posterior areas, compared to anterior and inferior areas. The curves of mean diffusivity vs. age of HD participants within a fixed CAP score were different from those of controls, indicating that the disease has an additional effect to age on the microscopic brain structure. These results show the regional and temporal vulnerability of the white matter and deep gray matter in HD, with potential implications for experimental therapeutics.

1. Introduction

Huntington's disease (HD) is a degenerative disease that classically manifests with motor, cognitive and behavioral features (Ross, 2014; Tabrizi et al., 2020). The diagnosis is based on the assessment of motor signs using the unified Huntington's disease rating scale (UHDRS) (Kremer et al., 1996) and cognitive deficits (Ross et al., 2019). HD is caused by a CAG repeat expansion in the Huntingtin gene (HTT) on chromosome 4, which codes for polyglutamine in the Huntingtin protein (Htt). Longer CAG repeat length has been associated to early HD onset (Brinkman et al., 1997). The so called "CAP" score, a product of the CAG repeat length and the individual's age (Ross, 2014; Zhang, 2011) is accepted as an index of the extent of exposure to the CAG expansion mutation.

While HD has traditionally been noted for selective striatal neurodegeneration (Vonsattel, 1985); there are increasing evidences that many other regions of the brain are affected (Rüb, 2016) in different stages of the disease, and in multiple ways other than atrophy. Early single-site and more recent multicenter studies (Aylward et al., 2013; Paulsen, 2014; Tabrizi, 2013; Dominguez, 2016) showed progressive striatal atrophy many years prior to the onset of motor symptoms, associated with subcortical white matter atrophy (Novak et al., 2014;

* Corresponding author.
E-mail address: afaria1@jhmi.edu (A.V. Faria).

https://doi.org/10.1016/j.nicl.2023.103493
Received 1 December 2022; Received in revised form 29 April 2023; Accepted 7 August 2023
Available online 9 August 2023

Paulsen, 2006; Stoffers et al., 2010). Previous diffusion tensor image (DTI) studies indicated white matter abnormalities in the corpus callosum (Crawford et al., 2013), internal capsule (Rosas, 2006), corticospinal tract (Phillips et al., 2015); cortico-striatal circuit (Novak et al., 2014), and extensively distributed in the white matter (Novak et al., 2014; Reading et al., 2005; Faria et al., 2016; Wu et al., 2016; Zhang et al., 2018) years before symptoms occur. Reduction in fractional anisotropy (FA) and increase in mean diffusivity (MD), which may be related to the disruption of white matter integrity and the increase of tissue water content (Winklewski et al., 2018; Orth et al., 2016), were consistently reported.

Although the previous studies have been insightful, they used different analytic methods, and have emphasized different hypothesis and results. Furthermore, several studies focused in specific regions of interest, and did not use large multi-center datasets (Georgiou-Karistianis, 2013; Tan, et al., 2022) (see (Gatto and Weissmann, 2019; van de Zande et al., 2022) for reviews). With the advances in automated imaging processing and analysis, and the accumulation and sharing of data from multicenter studies, we are now able to analyze large datasets together (Müller et al., 2011; Müller, 2013); across a range of CAP scores, using a fully automated and data driven approach (Steventon et al., 2016). We traced the longitudinal evolution of DTI indices, as a reflection of the white matter tissue status through PREDICT-HD and IMAGE-HD datasets. We found dramatic changes correlating with CAP scores, particularly in mean diffusivity, involving, but not restricted to, the basal ganglia circuit. We used change-point analysis to assess the "inflection points" in which the changes accelerate. We then evaluated the influence of the disease, versus sole age effect, in the evolution of DTI metrics.

2. Methods

2.1. Datasets

The datasets were obtained from two multicenter longitudinal studies, PREDICT-HD (Paulsen, 2006) and IMAGE- HD (Poudel, 2015), through CHDI (https://chdifoundation.org/). From PREDICT-HD, 463 HD participants with "premanifest" disease at study entry (i.e., before symptoms onset) and 159 healthy controls were included. From IMAGE-HD, 72 HD participants (both premanifest and manifest HD participants at entry) and 35 controls were included. The demographic characteristics of participants included in this study (after quality control exclusions, described in the Supplementary Table 1) are shown in Table 1.

Since the datasets have proportionally less very far-from-onset HD participants, we instead used controls as surrogates for them. This is supported by studies showing gene carriers very far from onset (about 20 years) have image metrics essentially equivalent to normal (Scahill, 2020); and the first differences in fiber density are reported about 10 years before onset (Zeun, et al., 2021). We note that, if HD is a neurodevelopmental disease (van der Plas et al., 2019; van der Plas et al., 2020; Meng et al., 2017; Pérot, 2022), the controls' data should be interpreted as reflecting a combination of developmental differences, plus the major component of degeneration. To help spreading the control's data out over a larger range of CAP scores (Liu, 2022), CAG repeats = 39.2 were used for controls, in the formula CAP = Age*(CAG-33.66) (Zhang, 2011). Although this is arbitrary, it is based on the fact that, while the HD phenotype is not always penetrant in individuals with 36 to 39 repeats (Kremer, 1994; Rubinsztein, 1996), higher disease repeats are virtually always associated to individuals who will develop HD pathology (Maat-Kievit et al., 2001; Langbehn, 2004), which the controls are surrogates for.

2.2. Image processing

The 3T MRIs were automatically segmented and postprocessed through MRICloud (https://www.MRICloud.org) (Mori, 2016), a public web-based service for multi-contrast imaging segmentation and quantification. The DTI tensor reconstruction and quality control followed the algorithm used by DtiStudio (https://www.MRIStudio.org). The DTI segmentation involved image mapping based on a sequence of linear algorithms and Large Deformation Diffeomorphic Mapping (LDDMM) (Ceritoglu et al., 2013), using complementary contrasts (mean diffusivity [MD], fractional anisotropy [FA], and the eigenvector that indicates fiber orientation), and a final step of multi-atlas labeling fusion (Tang et al., 2013; Tang et al., 2014).

The original images along with the results of the brain segmentation obtained from MRICloud were visually inspected for quality control. The image quality control leaded to the exclusion of 42 PREDICT- HD scans (14 from control group and 28 from HD group, specifically 16 high-CAP, 8 medium-CAP, 4 low-CAP, according to the criteria in (Zhang, 2011), and 2 IMAGE-HD scans (1 control, 1 HD). This corresponds to approximately 2.8% of our datasets. The reasons for exclusion were: incomplete brain coverage and/or errors in the initial linear image registration (21 scans),'ghost' effect and other technical corruption artifacts (19 scans), motion artifacts (4 scans: 3 controls and 1 HD high-CAP). We additionally excluded 7 PREDICT scans with unconfirmed CAP scores. Please note that Table 1 shows only the data used in this study, therefore after the quality control exclusions. Human correction of the segmentation was avoided, as the aim is to report the results of a consistent automated process across all the images.

Table 1
Demographic characterstics of participants in the PREDICT-HD and IMAGE-HD datasets used in this study.

	PREDICT-HD (n = 622, 1247 scans)		IMAGE-HD (n = 107, 253 scans)	
	HD (n = 463, 893 scans)	Controls (n = 159, 354 scans)	HD (n = 72, 169 scans)	Controls (n = 35, 84 scans)
Age	42.8 ± 12.1 [18.6–77.6]	47.5 ± 12.1 [23.2–85.7]	47.0 ± 11.1 [23.9–73.4]	43.2 ± 13.9 [24.4–73.0]
CAP*	353.1 ± 100.1 [79.1–721.6]		408.4 ± 90.6 [163.3–632.9]	
low - mid - high CAP*	124–139 –200		6–19 – 47	
CAG repeats	42.3 ± 2.8 [36.0–62.0]		42.6 ± 2.2 [39.0–50.0]	
UHDRS-TMS	8.6 ± 10.9 [0.0–69.0]	3.6 ± 4.3 [0.0–25.0]	10.1 ± 13.9 [0.0–74.0]	
SDMT	50.3 ± 11.6 [6.0–81.0]	53.6 ± 10.3 [26.0–95.0]	44.7 ± 13.1 [15.0–74.0]	56.0 ± 10.0 [31.0–80.0]
BDI	7.1 ± 6.9 [0.0–26.0]	5.1 ± 6.3 [0.0–29.0]	7.7 ± 8.3 [0.0–39.0]	3.9 ± 4.1 [0.0–16.0]
Sex, female/ male (%)	307 / 156 (66.3%/ 33.7%)	100 / 59 (62.9%/ 37.1%)	37 / 35 (51.4%/ 48.6%)	23 / 12 (65.7%/ 34.3%)
Participants with 1–7 time points	217, 131, 66, 35, 9, 4, 1	60, 43, 28, 17, 10, 1, 0	15, 17, 40, 0, 0, 0, 0	7, 7, 21, 0, 0, 0, 0
Participants with manifested HD, manifested HD during the study	41, 28		14, 14	

Note: UHDRS represents Unified Huntington's Disease Rating Scale; TMS represents Total Motor Score; SDMT represents Symbol-Digit Modalities Test; BDI represents Beck Depression Inventory. *CAP scores and cut-offs for low - med - high groups as in (Zhang, 2011).

2.3. Regions and metrics analyzed

The deep gray matter and whole brain white matter were automatically segmented, in regions of interest (ROIs) defined in digital white matter atlases (Oishi et al., 2009; Mori et al., 2009). These ROIs were putamen, caudate nucleus, globus pallidus, thalamus, anterior, posterior and superior corona radiata, anterior and posterior limb internal capsule, corpus callosum, cerebral peduncle, inferior fronto-occipital fasciculus, middle cere- bellar peduncle, posterior thalamic radiation, retrolenticular internal capsule, sagittal stratum, superior longitudinal fasciculus, and uncinate fasciculus. The superficial white matter considered were areas with FA > 0.25 beneath the following gyri: superior, middle and inferior frontal, temporal and occipital, superior parietal, post-central, pre-central, angular, supramarginal, fusiform, cuneus, pre-cuneus, lingual, lateral and middle fronto-orbital, rectus, insula and cingulate. We also analyzed the cerebellar white matter. ROIs in both hemispheres were considered together as there is is little evidence for significant asymmetry in HD (Rosas et al., 2002; Klöppel et al., 2008). Brainstem was not included because the variable level of scan coverage could introduce artifact variations (Vaswani, 2017).

At each voxel, the DTI defines a diffusion tensor composed of three orthogonal eigenvectors and respective eigenvalues (λ_1, λ_2 and λ_3, in descending order of amplitude). The following metrics were analyzed in this study: 1) Axial Diffusivity (AD, or λ_1), which describes the rate of diffusion along the orientation of the fibers; 2) Radial Diffusivity (RD, the mean of λ_2 and λ_3), which is proportional to the diffusion magnitude in the plane perpendicular to the axon bundles. 3) Trace (the sum of λ_1, λ_2 and λ_3) which is proportional to the mean diffusivity, MD (which is trace / 3); and 4) Fractional Anisotropy (FA, similar to the standard deviation of λ_1, λ_2 and λ_3, ranging from 0 to 1), which is proportional to the diffusion asymmetry within a voxel. Based on seminal studies (Beaulieu and Allen, 1994; Beaulieu and Allen, 1994; Moseley et al., 1991; Gulani et al., 2001; Takahashi, 2002; Kinoshita et al., 1999), AD has been accepted as indicator of axional damage; RD is correlated with myelin damage; MD possibly reflects structural integrity as well as FA, which is also an indicator of fiber density, axonal organization and myelination. Although our study cannot define the cellular bases of these metrics, it can help map the topography of possible abnormalities.

2.4. Statistical models

Two models, a linear fitting and a left-flat sigmoidal function (as defined in (Liu, 2022), were implemented to capture the changes in DTI metrics in each ROI over CAP scores. We chose the sigmoidal model based on previous work characterizing age differences and longitudinal changes of diffusion MRI metrics (Beck et al., 2021; Benitez et al., 2018; Falangola, 2008; Jelescu, 2015; Kodiweera et al., 2016; Westlye et al., 2010; Faria et al., 2010), and our previous analysis of volumetric changes in HD (Liu, 2022). Through these studies, we expected curvilinear relationships with age and CAPs, with varying trajectories and deflection points possibly reflecting differential involvement and rate of change of the putative biological underpinnings during the different phases of the disease. We statistically tested the sigmoidal models against linear models to find whether, and for which structure, they provide a better reflection of the progressive, but expected non-linear, nature of neurodegeneration in HD.

These are hybrid models that consider a combination of within-subject and between-subject effects. The models assumed that far from the disease onset (low CAP) HD brains are indistinguishable from healthy controls brains. The source of data (PREDICT-HD or IMAGE-HD) and the subject group (control or HD) were models' covariates. For the ROIs in which the sigmoidal model was significantly different from the linear model (p-value < 0.05, corrected for multiple comparisons with FDR (Benjamini and Hochberg, 1995), a "change-point" was inferred from the sigmoidal regression models, similar to (Wu et al., 2017). The change-point indirectly indicates the point (CAP score) in which changes in brain anatomy (DTI indices) become greater (i.e., where the fitting curve pass through the "flat" part to the "steep" part). The variance of the change-point was assessed via parametric bootstrap with 1000 folds. The construction of the statistical regression models was carried out using Python 3.7.

An additional important question is whether the changes of DTI indices over time reflect only natural aging (Beck et al., 2021; Benitez et al., 2018; Falangola, 2008; Jelescu, 2015; Kodiweera et al., 2016; Westlye et al., 2010), or if there are additional effects of the disease. To answer this question, we compared 173 HD participants in a tight range of CAG repeats with a group of 159 controls paired in age and sex (Table 2). Differences between the curves of DWI indices in each ROI versus age were accessed with Chow test (Chow, 1960), corrected for multiple comparisons with FDR (Benjamini and Hochberg, 1995).

3. Results

For most of brain areas and DTI metrics, the left-flat sigmoidal fitting did not differ significantly from the linear fitting. Therefore, for most of brain areas, the results of the simplest model (linear) are shown. Exceptions were trace, AD, and RD in the deep gray and deep white matter (Fig. 1; the individual "spaghetti plots" that generated those curves, per metric and per ROI, are in Supplementary Material). In these areas, the evolution of the DTI indices (except FA) over CAP scores followed sigmoidal curves better than linear ones, with DTI indices showing a plateau at low CAP scores, then drastically increasing. Table 3 shows the change-points estimated with the sigmoidal curves. These change-points are graphically represented in Fig. 3. In general, for each ROI, the change-points occurred within a similar time frame for trace, MD and AD. The change-point was earlier (i.e., at lower CAP scores) in the deep gray matter (putamen and globus pallidus) than in the deep white matter (superior corona radiata and sagittal stratum).

Table 4 shows the linear models' slopes and r-squared in the ROIs and metrics for which the sigmoidal fitting did not differ from the linear fitting (so we favoured to present the results of the simplest model) (see Fig. 4 for graphic illustration). The complete description of the linear parameters, for all the regions and metrics, is shown in the supplementary materials. Similar to the change-points, we observed a general tendency of more conspicuous changes (highest slopes and r-squared) in the deep gray matter, followed by corpus callosum and thalamus, then deep white matter, and peripheral white matter at last. Within the white matter, posterior and superior structures (e.g., posterior thalamic radiations and superior corona radiata within the deep white matter, and occipital and parietal areas within the peripheral white matter) tended to have more conspicuous changes in trace, RD, and MD. The FA had an inverse relationship with CAP scores (as expected) and was the least sensitive index, with the largest number of ROIs showing no significant change of FA over CAP scores.

The curves of DTI indices vs. age of HD participants (CAG 41–42) were significantly different from those of controls in the majority of the deep gray and white matter ROIs as shown in Table 4 and illustrative spaghetti plots in Fig. 2 (other spaghetti plots are in the supplementary material). This indirectly indicates that the disease plays a role in the evolution of DTI indices, in addition to the natural aging. The trace, RD and AD curves were even less similar between HD and controls, compared to the FA curves. This again provides evidences that FA may be less sensitive than the other DTI indices to the HD time course.

Table 2
Demographic characteristics of subjects in control and HD groups used for the comparisons between curves of DTI indices vs. age.

	Age Range (Mean)	Gender Distribution (%)	Number of Scans
Controls (n = 159)	23.2–85.7 (47.5)	F: 100 (62.9%) M: 59 (37.1%)	354
HD (41–42 CAG; n = 173)	18.8–75.9 (43.5)	F: 110 (63.6%) M: 63 (36.4%)	338

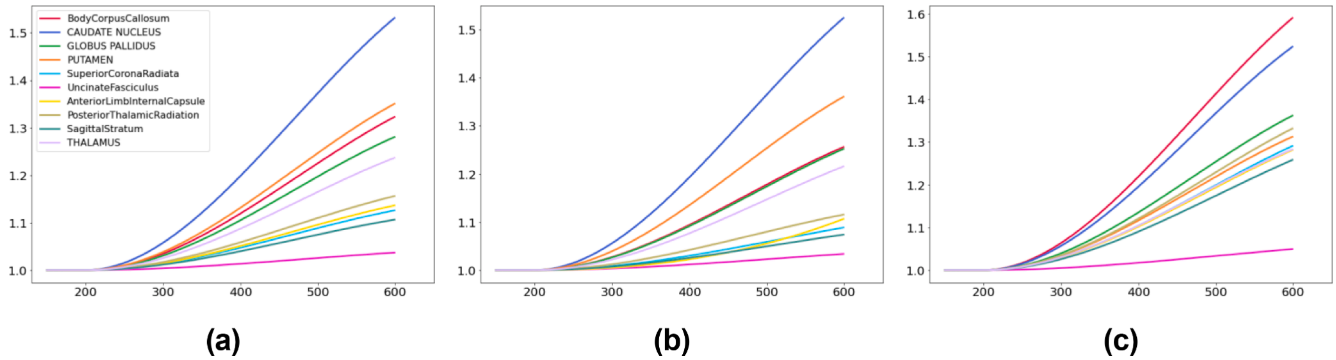

Fig. 1. Sigmoidal curve fitting of (a) Trace, (b) Radial Diffusivity, (c) Axial Diffusivity (y-axis) over CAP scores (x-axis), for different brain structures (color-coded). Y-axis presents the fitted diffusivity indices normalized by the smallest fitted value for each structure. This normalization makes all the curves comparable, with the same starting points, and was used only for visualization.

Table 3
Change points of diffusivity indices in the deep gray and white matter.

ROI	RD			AD			Trace		
	t0	SD	p-value	t0	SD	p-value	t0	SD	p-value
Body Corpus Callosum	320	29	<0.01	326	29	<0.01	324	29	<0.01
Caudate	329	26	<0.01	328	25	<0.01	328	24	<0.01
Globus Pallidus	233	44	<0.01	242	53	0.01	223	45	<0.01
Putamen	247	44	<0.01	272	44	<0.01	252	43	<0.01
Superior Corona Radiata	272	30	0.02	201	37	0.02	253	24	0.01
Uncinate Fasciculus	405	35	<0.01	365	41	0.02	331	41	0.04
Anterior Limb Internal Capsule	292	43	<0.01	257	39	0.06*	286	34	<0.01
Posterior Thalamic Radiation	269	49	0.02	347	53	0.04	363	56	0.08*
Sagittal Stratum	259	43	0.01	242	44	0.43*	249	35	0.04
Thalamus	319	38	0.02	290	47	0.27*	329	41	0.02

Note: * indicates no significant difference between sigmoidal and linear models fitting the specific DTI index over CAP scores in the region in question. The results are still presented in this table for the sake of consistency.

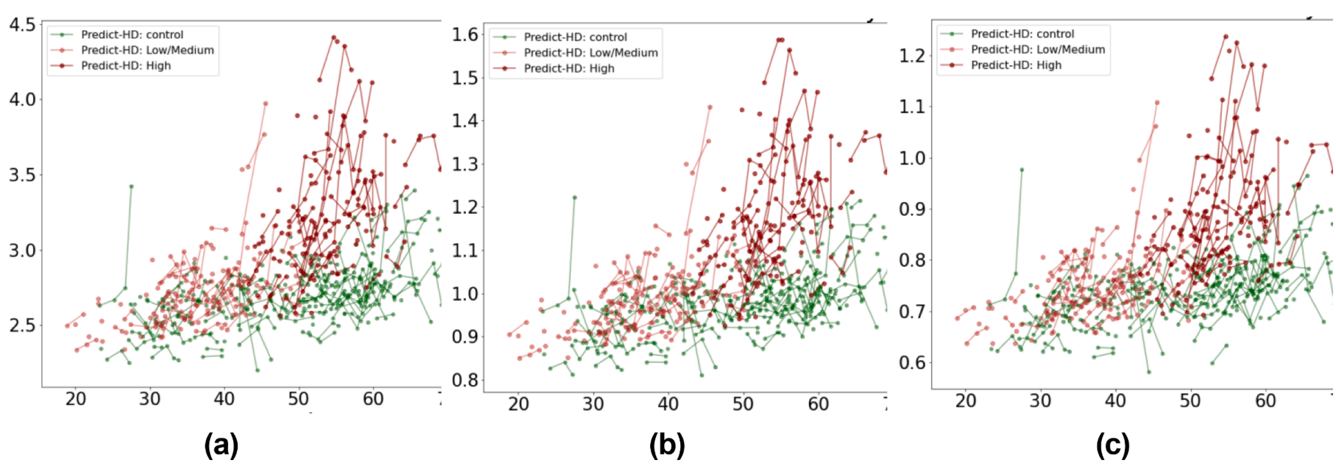

Fig. 2. Illustrative spaghetti plots of (a) Trace, (b) Radial Diffusivity, (c) Axial Diffusivity (y-axis, values $\times 10^4$) versus age (x-axis), for controls and HD participants (CAG repeats 41–42) in caudate.

4. Discussion

We traced the longitudinal evolution of DTI metrics in HD aiming to describe a regional or temporal vulnerability pattern of potential relevance for future therapeutic design. In agreement with previous studies (see (Estevez-Fraga et al., 2021) for a review) our results showed longitudinal changes in DTI indices in most regions of the brain. Although this is expected according to the natural aging process (Westlye et al., 2010; Salat, 2005; Lebel et al., 2012; Behler et al., 2021; Bethlehem, 2022), the comparison of curves of HD participants, in a restricted range of CAG repeat with age-paired controls, indicated widespread differences, therefore highlighting an additional significant disease effect. As in other neurodegenerative diseases, there were longitudinal increases in diffusivity metrics (i.e., trace, RD, AD) and a decrease in FA (Gatto and Weissmann, 2019; van de Zande et al., 2022) (except in predominantly gray matter structures, in which FA longitudinally increases (Pfefferbaum et al., 2010); potentially reflecting loss of neurons and/or connections and therefore a "simplification" of the fiber composition (Estevez-Fraga et al., 2021). The trace was more sensitive than FA (which is more affected by the image noise (Pierpaoli and Basser, 1996; Magnotta et al., 2012), indicating that HD is likely to cause disturbances of the microstructural organization that are more

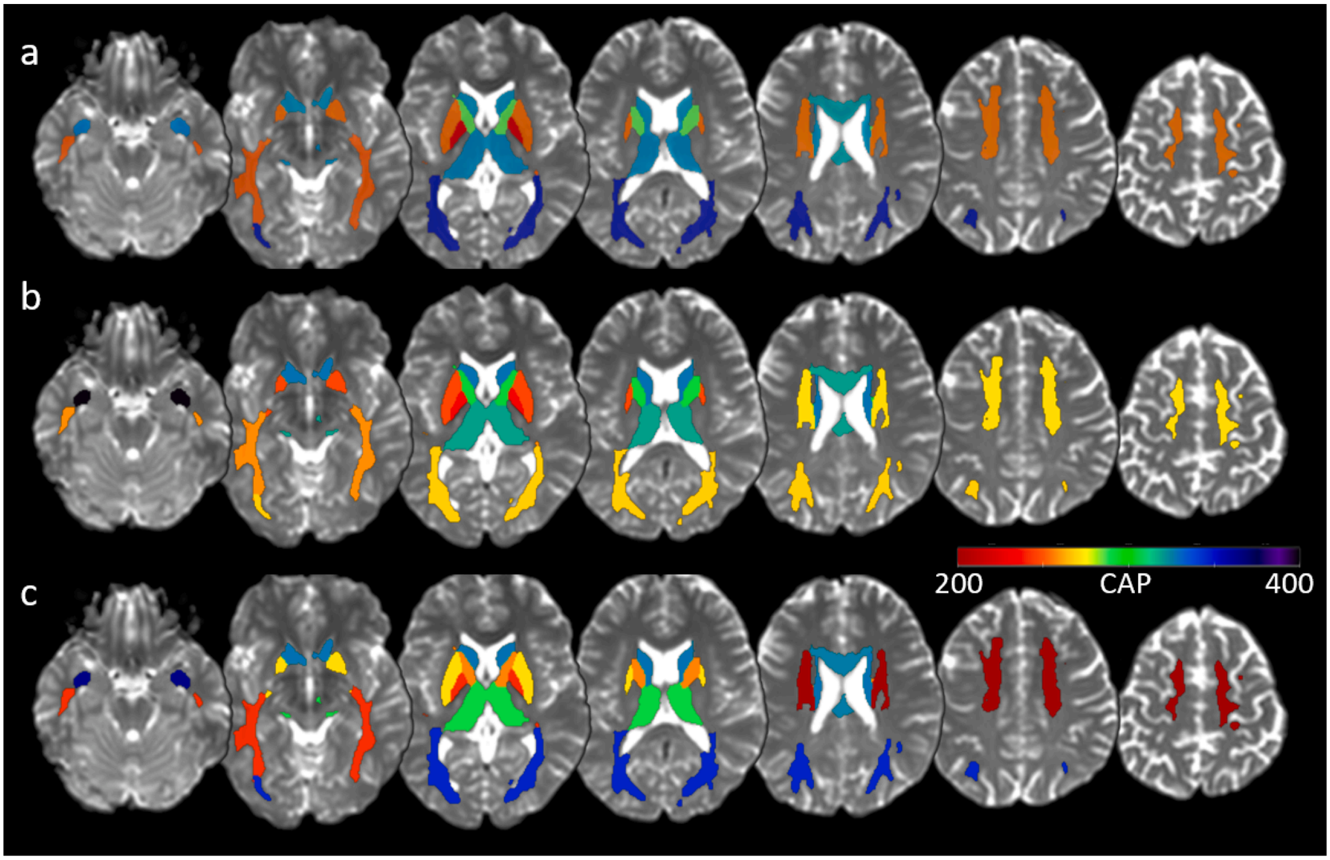

Fig. 3. "Change-points" (color coded over an anatomical brain image) from the sigmoid curves of CAP scores vs. DTI indices (trace (a), radial diffusivity, RD (b), axial diffusivity, AD (c)). For example, in a green-coded area, the inflection of the sigmoid fitting curve (between the "flat" left portion and the "steep" right portion) occurs around CAP score 300. (For interpretation of the references to color in this figure legend, the reader is referred to the web version of this article.)

sensitively detected by MD than by FA measurements.

The deep gray matter and the deep white matter areas, such as superior corona radiata and sagittal stratum, tended to be affected in earlier stages (i.e., at lower CAP scores), compared to peripheral areas, such as the white matter beneath the lingual and middle occipital gyri. This is possibly due to a combination of biological and technical effects. Technically, the peripheral white matter areas are more susceptible to image noise and mapping inaccuracies (Snook et al., 2007). Note, for instance, the higher variability of all four DTI metrics in the peripheral compared to core white matter in the Supplementary Material spaghetti plots. Biologically, it is reasonable to ascertain that changes in deep areas occur first and more dramatically than in peripheral areas. This agrees with the sequence of atrophy observed in brain structures, showed by multicenter longitudinal studies (Liu, 2022) and simulations, (Wijeratne et al., 2021) that atrophy in basal ganglia circuit including caudate, putamen, globus pallidus is more dramatic compared with other regions (i.e., superior frontal and superior temporal white matter) which are generally steady and slower.

This gradient of changes also agrees with our previous observations in a smaller dataset (Faria et al., 2016; Wu et al., 2017), that the evolution of diffusivity indices seem to follow a centripetal and posterior-anterior temporal gradient, in which mesial and posterior white matter areas show changes in DTI indices earlier than inferior and anterior areas. For instance, superior corona radiata and sagittal stratum presented earlier "change points" than anterior limb of internal capsule and uncinate fasciculus. This observation also indirectly aligns with the theory of spread of pathology from the basal ganglia circuit to other parts of the brain (Ross, 2014).

The strengths of this study include the analysis of two large and multicenter datasets, with a total of 729 participants in multiple time points. The combination of different datasets and inclusion of heterogeneous data enhances the potential generalization of the results. We adopted the same automated, data-driven approach to automatically process a large number of DTIs, increasing the robustness of our findings and enabling further reproducibility studies. In addition, the population has a wide range of CAP scores, with most participants in premanifest period, a relatively early stage of HD.

There are, however, several limitations. There are possible inaccuracies on brain segmentation, particularly in regions with low contrast, that are more liable to higher variation on the boundary definition. We did not make manual corrections on individual basis, first because the variability on brain segmentation is an issue faced by humans as well, and second because we wanted to keep the methodology completely automated, reproducible, and feasible to other 'Big Data' studies. Therefore, the results must be interpreted in the light of the regional segmentation reliability (Rezende, 2019). The DWI protocols were homogenized as much as possible among the different centers that participated of PREDICT and Image-HD. However, it is impossible to eliminate all the residual differences in data from different centers and scanners. Although we included the study source as a covariant of our models, the lack of effective harmonization for all the possible image parameters may increase the data variance and the risk of false negative results. Moreover, the current study benefits from a mixed cross-sectional and longitudinal design, where participants can be used as their own baseline (Sexton, 2014). However, the main results were largely driven by the cross-sectional data, whose samples dominate the longitudinal one. Finally, we artificially used controls as surrogates for very far-from-onset HD subjects. This has to be taken with caution, particularly considering the hypothesis of HD as a neurodevelopmental disease, which would make the groups not comparable.

Table 4
P-value of the comparisons between curves of DTI indices vs. age, for controls and HD individuals (CAG repeat 41–42) groups, age-balanced.

ROI	FA	AD	RD	Trace
Anterior Corona Radiata	2.08×10^{-4}	2.93×10^{-12}	3.39×10^{-10}	1.48×10^{-11}
Anterior Limb Internal Capsule	6.91×10^{-4}	1.98×10^{-13}	1.83×10^{-8}	4.42×10^{-11}
Body Corpus Callosum	1.11×10^{-16}	1.11×10^{-16}	1.11×10^{-16}	1.11×10^{-16}
Caudate	8.31×10^{-5}	1.11×10^{-16}	1.11×10^{-16}	1.11×10^{-16}
Cerebral Peduncle	1.31×10^{-2}	7.64×10^{-6}	3.94×10^{-4}	3.14×10^{-5}
Corticospinal Tract	9.29×10^{-1} *	8.02×10^{-1} *	4.17×10^{-1} *	6.44×10^{-1} *
Globus Pallidus	7.18×10^{-2} *	7.08×10^{-14}	1.11×10^{-16}	1.11×10^{-16}
Inferior Fronto-occipital Fasciculus	1.48×10^{-1} *	1.81×10^{-8}	1.01×10^{-12}	4.62×10^{-13}
Middle Cerebellar Peduncle	1.59×10^{-4}	3.64×10^{-4}	1.76×10^{-1} *	5.17×10^{-2} *
Posterior Corona Radiata	3.40×10^{-2} *	2.87×10^{-9}	1.92×10^{-13}	4.12×10^{-13}
Posterior Limb Internal Capsule	6.37×10^{-1} *	1.89×10^{-3}	9.70×10^{-4}	3.16×10^{-4}
Posterior Thalamic Radiation	1.35×10^{-5}	1.11×10^{-16}	1.11×10^{-16}	1.11×10^{-16}
Putamen	3.46×10^{-13}	1.11×10^{-16}	1.11×10^{-16}	1.11×10^{-16}
Retrolenticular Internal Capsule	8.12×10^{-1} *	1.20×10^{-7}	3.33×10^{-16}	2.44×10^{-15}
Sagittal Stratum	4.54×10^{-5}	9.84×10^{-13}	1.38×10^{-10}	1.38×10^{-12}
Superior Corona Radiata	1.22×10^{-5}	2.96×10^{-9}	1.47×10^{-6}	6.42×10^{-8}
Superior Longitudinal Fasciculus	4.22×10^{-3}	2.98×10^{-10}	1.34×10^{-13}	1.55×10^{-13}
Thalamus	4.89×10^{-4}	1.11×10^{-16}	1.11×10^{-16}	1.11×10^{-16}
Uncinate Fasciculus	9.43×10^{-2} *	1.85×10^{-5}	1.58×10^{-11}	5.06×10^{-10}

Note: * indicates no significant difference between curves of controls and HD after correction for multiple comparisons.

Regardless of all these limitations, these data provide a comprehensive description of the natural history of regional microscopic brain structures in HD. They highlight the widespread degeneration of many regions of the brain including white matter, which is consistent with studies showing that not just neurons but other cells can contribute to HD pathogenesis (Creus-Muncunill and Ehrlich, 2019). They also highlight the predominant influence on regions in the basal ganglia circuit with implications for pathogenesis (Poudel et al., 2019; Rüb et al., 2014; Waldvogel et al., 2015) and experimental therapeutics. For example, these results support the hypothesis of circuit-based spread of pathology in HD, possibly due to the spread of mutant Htt protein (Cicchetti et al., 2014; Gosset et al., 2020; Lee, 2020; Pecho-Vrieseling, 2014; Masnata et al., 2019) or other mechanisms such as loss of growth factor transport, or altered synaptic connectivity (Virlogeux et al., 2018; Saudou and Humbert, 2016), perhaps due to abnormal complement-mediated pruning (Liddelow et al., 2017). They indirectly imply the search for novel therapeutic targets related to prion-like spread of pathology, and for modifications in therapeutic approaches solely focused on the caudate and putamen, which misses other early affected brain structures.

In conclusion, this study spans key stages of HD and represents the most comprehensive delineation of the natural history of regional brain changes in DTI metrics to date. It provides a detailed overview of how DTI metrics change over the progression of HD, shedding light to potential markers for understanding the natural history of HD, and for designing of experimental therapeutics.

Data Availability

The datasets used in this study are available from the study authors coordinators (IMAGE-HD: NGK; PREDICT-HD: JSP) under a suitable data sharing agreement.

Funding

We would like to acknowledge the contribution of all the participants who took part in this study. ImageHD is grateful to the CHDI Foundation Inc. (grant number A – 3433), New York (USA), and to the National Health and Medical Research Council (NHMRC) (grant number 606650) for their funding; and the Royal Children's Hospital for the use of their 3 T MR scanner. This study was supported by the National Institute of

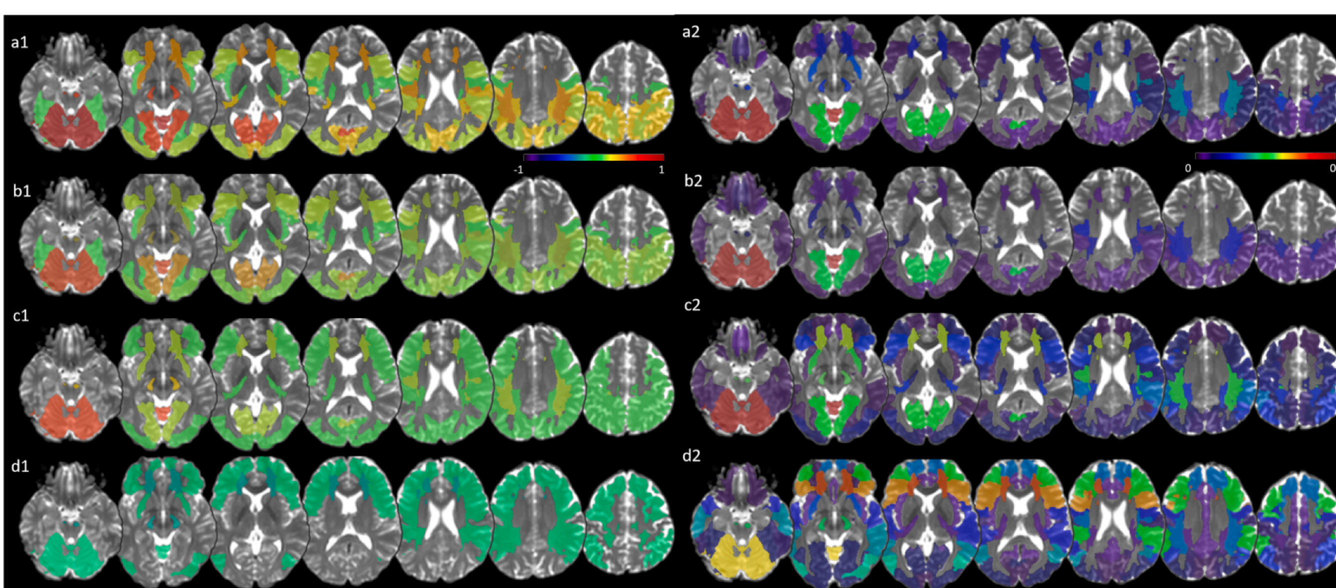

Fig. 4. Color-coded parameters of the linear models (slopes in left panel 1, r-squared in right panel 2) in brain regions that showed no significant differences between sigmoidal and linear models (so linear parameters are shown). Slopes for (a) trace, (b) radial diffusivity, RD, (c) axial diffusivity, AD, and (d) FA are $\times 10^{3}$.

Neurological Disorders and Stroke, NINDS, NS102670-01A1, and by the National Institute of Biomedical Imaging and Bioengineering, NIBIB, P41EB031771. We thank CHDI for maintaining and transmitting (Darren Freeman) the datasets for these analyses.

Author contribution

AVF and BH conceived and designed the study, interpreted the data, and drafted the work. BH and HL collected and analyzed the data. XB performed the images quality control. LY developed the statistical method and guided the statistical analysis. JP and NGK provided the data and contributed to the final draft of the paper. TR and CR reviewed the draft.

Declaration of Competing Interest

MIM owns a founder share of Anatomy Works with the arrangement being managed by Johns Hopkins University in accordance with its conflict-of-interest policies. All the authors, including MIM, have no financial interests or personal relationships that could have appeared to influence the work reported in this paper.

Data availability

Data will be made available on request.

Appendix A. Supplementary data

Supplementary data to this article can be found online at https://doi.org/10.1016/j.nicl.2023.103493.

References

Aylward, E.H., Harrington, D.L., Mills, J.A., Nopoulos, P.C., Ross, C.A., Long, J.D., Liu, D., Westervelt, H.K., Paulsen, J.S., 2013. Regional atrophy associated with cognitive and motor function in prodromal huntington disease. J. Huntington's Disease 2 (4), 477–489.

Beaulieu, C., Allen, P.S., 1994. Water diffusion in the giant axon of the squid: implications for diffusion- weighted mri of the nervous system. Magn. Reson. Med. 32, 579–583.

Beaulieu, C., Allen, P.S., 1994. Determinants of anisotropic water diffusion in nerves. Magn. Reson. Med. 31 (4), 394–400.

Beck, D., de Lange, A.-M., Maximov, I.I., Richard, G., Andreassen, O.A., Nordvik, J.E., Westlye, L.T., 2021. White matter microstructure across the adult lifespan: A mixed longitudinal and cross-sectional study using advanced diffusion models and brain-age prediction. NeuroImage 224, 117441.

Behler, A., Kassubek, J., Müller, H.-P., 2021. Age-related alterations in dti metrics in the human brain—consequences for age correction. Front. Aging Neurosci. 13.

Benitez, A., Jensen, J.H., Falangola, M.F., Nietert, P.J., Helpern, J.A., 2018. Modeling white matter tract integrity in aging with diffusional kurtosis imaging. Neurobiol. Aging 70, 265–275.

Benjamini, Y., Hochberg, Y., 1995. Controlling the false discovery rate: a practical and powerful approach to multiple testing. J. Royal Stat.. Soc.: Ser. B (Methodological) 57, 289–300.

Bethlehem, R.A., et al., 2022. Brain charts for the human lifespan. Nature 1–11.

Brinkman, R., Mezei, M., Theilmann, J., Almqvist, E., Hayden, M., 1997. The likelihood of being affected with huntington disease by a particular age, for a specific cag size. Am. J. Human Gen. 60, 1202.

Ceritoglu, C., Tang, X., Chow, M., Hadjiabadi, D., Shah, D., Brown, T., Burhanullah, M. H., Trinh, H., Hsu, J.T., Ament, K.A., Crocetti, D., Mori, S., Mostofsky, S.H., Yantis, S., Miller, M.I., Ratnanather, J.T., 2013. Computational analysis of lddmm for brain mapping. Front. Neurosci. 7.

Chow, G.C., 1960. Tests of equality between sets of coefficients in two linear regressions. Econom. J. Econom. Soc. 28 (3), 591.

Cicchetti, F., Lacroix, S., Cisbani, G., Vallières, N., Saint-Pierre, M., St-Amour, I., Tolouei, R., Skepper, J.N., Hauser, R.A., Mantovani, D., Barker, R.A., Freeman, T.B., 2014. Mutant huntingtin is present in neuronal grafts in huntington disease patients. Ann. Neurol. 76 (1), 31–42.

Crawford, H.E., Hobbs, N.Z., Keogh, R., Langbehn, D.R., Frost, C., Johnson, H., Landwehrmeyer, B., Reilmann, R., Craufurd, D., Stout, J.C., Durr, A., Leavitt, B.R., Roos, R.A.C., Tabrizi, S.J., Scahill, R.I., 2013. Corpus callosal atrophy in premanifest and early huntington's disease. J. Huntington's disease 2 (4), 517–526.

Creus-Muncunill, J., Ehrlich, M.E., 2019. Cell-autonomous and non-cell-autonomous pathogenic mech- anisms in huntington's disease: insights from in vitro and in vivo models. Neurotherapeutics 16 (4), 957–978.

Dominguez, J.F., et al., 2016. Multimodal imaging biomarkers in premanifest and early huntington's disease: 30-month image-hd data. The Br. J. Psychiatry 208, 571–578.

Estevez-Fraga, C., Scahill, R., Rees, G., Tabrizi, S.J., Gregory, S., 2021. Diffusion imaging in huntington's disease: comprehensive review. J. Neurol. Neurosurg. Psychiatry 92, 62–69.

Falangola, M.F., et al., 2008. Age-related non-gaussian diffusion patterns in the prefrontal brain. J. Magn. Reson. Imaging: An Off. J. Int. Soc. for Magn. Reson. Medicine 28, 1345–1350.

Faria, A.V., Zhang, J., Oishi, K., Li, X., Jiang, H., Akhter, K., Hermoye, L., Lee, S.-K., Hoon, A., Stashinko, E., 2010. Atlas-based analysis of neurodevelopment from infancy to adulthood using diffusion tensor imaging and applications for automated abnormality detection. NeuroImage 52 (2), 415–428.

Faria, A.V., Ratnanather, J.T., Tward, D.J., Lee, D.S., van den Noort, F., Wu, D., Brown, T., Johnson, H., Paulsen, J.S., Ross, C.A., Younes, L., Miller, M.I., 2016. Linking white matter and deep gray matter alterations in premanifest huntington disease. Neuroimage: clinical 11, 450–460.

Gatto, R.G., Weissmann, C., 2019. Diffusion tensor imaging in preclinical and human studies of huntington's disease: what have we learned so far? Curr. Med. Imaging 15, 521–542.

Georgiou-Karistianis, N., et al., 2013. Automated differentiation of pre-diagnosis huntington's disease from healthy control individuals based on quadratic discriminant analysis of the basal ganglia: the image-hd study. Neurobiol. disease 51, 82–92.

Gosset, P., Maxan, A., Alpaugh, M., Breger, L., Dehay, B., Tao, Z., Ling, Z., Qin, C., Cisbani, G., Fortin, N., Vonsattel, J.-P., Lacroix, S., Oueslati, A., Bezard, E., Cicchetti, F., 2020. Evidence for the spread of human-derived mutant huntingtin protein in mice and non-human primates. Neurobiol. disease 141, 104941.

Gulani, V., Webb, A., Duncan, I., Lauterbur, P., 2001. Apparent diffusion tensor measurements in myelin- deficient rat spinal cords. Magn. Reson. Medicine: An Off. J. Int. Soc. for Magn. Reson. Medicine 45, 191–195.

Jelescu, I.O., et al., 2015. One diffusion acquisition and different white matter models: how does microstruc- ture change in human early development based on wmti and noddi? NeuroImage 107, 242–256.

Kinoshita, Y., Ohnishi, A., Kohshi, K., Yokota, A., 1999. Apparent diffusion coefficient on rat brain and nerves intoxicated with methylmercury. Environ. research 80, 348–354.

Klöppel, S. *et al.* White matter connections reflect changes in voluntary-guided saccades in pre- symptomatic huntington's disease. *Brain* **131**, 196–204 (2008).

Kodiweera, C., Alexander, A.L., Harezlak, J., McAllister, T.W., Wu, Y.-C., 2016. Age effects and sex differences in human brain white matter of young to middle-aged adults: A dti, noddi, and q-space study. NeuroImage 128, 180–192.

Kremer, B., et al., 1994. A worldwide study of the huntington's disease mutation: the sensitivity and specificity of measuring cag repeats. New Engl. J. Medicine 330, 1401–1406.

Kremer, H., Group, H. S. *et al.* Unified huntington's disease rating scale: reliability and consistency. *Mov. disorders* **11**, 136–142 (1996).

Langbehn, D.R., et al., 2004. A new model for prediction of the age of onset and penetrance for huntington's disease based on cag length. Clin. Genetics 65, 267–277.

Lebel, C., Gee, M., Camicioli, R., Wieler, M., Martin, W., Beaulieu, C., 2012. Diffusion tensor imaging of white matter tract evolution over the lifespan. NeuroImage 60 (1), 340–352.

Lee, C., et al., 2020. Disease-related huntingtin seeding activities in cerebrospinal fluids of huntington's disease patients. Sci. Reports 10, 1–14.

Liddelow, S.A., Guttenplan, K.A., Clarke, L.E., Bennett, F.C., Bohlen, C.J., Schirmer, L., Bennett, M.L., Münch, A.E., Chung, W.-S., Peterson, T.C., Wilton, D.K., Frouin, A., Napier, B.A., Panicker, N., Kumar, M., Buckwalter, M.S., Rowitch, D.H., Dawson, V. L., Dawson, T.M., Stevens, B., Barres, B.A., 2017. Neurotoxic reactive astrocytes are induced by activated microglia. Nature 541 (7638), 481–487.

Liu, C.-F., et al., 2022. Linking white matter and deep gray matter alterations in premanifest huntington disease. In Rev. Brain Commun.

Maat-Kievit, A., et al., 2001. New problems in testing for huntington's disease: the issue of intermediate and reduced penetrance alleles. J. medical genetics 38, e12–e.

Magnotta, V.A., Matsui, J.T., Liu, D., Johnson, H.J., Long, J.D., Bolster, B.D., Mueller, B. A., Lim, K., Mori, S., Helmer, K.G., Turner, J.A., Reading, S., Lowe, M.J., Aylward, E., Flashman, L.A., Bonett, G., Paulsen, J.S., 2012. Multicenter reliability of diffusion tensor imaging. Brain Connectivity 2 (6), 345–355.

Masnata, M., Sciacca, G., Maxan, A., Bousset, L., Denis, H.L., Lauruol, F., David, L., Saint-Pierre, M., Kordower, J.H., Melki, R., Alpaugh, M., Cicchetti, F., 2019. Demonstration of prion-like properties of mutant huntingtin fibrils in both in vitro and in vivo paradigms. Acta Neuropathologica 137 (6), 981–1001.

Meng, Y., Jiang, J., Bachevalier, J., Zhang, X., Chan, A.W., 2017. Developmental whole brain white matter alterations in transgenic huntington's disease monkey. Sci. Reports 7, 1–12.

Mori, S., et al., 2016. Mricloud: delivering high-throughput mri neuroinformatics as cloud-based software as a service. Comput. Sci. Eng. 18, 21–35.

Mori, S., Oishi, K., Faria, A.V., 2009. White matter atlases based on diffusion tensor imaging. Curr. Opinion Neurol. 22, 362.

Moseley, M.E., Kucharczyk, J., Asgari, H.S., Norman, D., 1991. Anisotropy in diffusion-weighted mri. Magn. Reson. Medicine 19, 321–326.

Müller, H.-P., et al., 2013. Evaluating multicenter dti data in huntington's disease on site specific effects: An ex post facto approach. NeuroImage: Clin. 2, 161–167.

Müller, H.-P., Glauche, V., Novak, M.J.U., Nguyen-Thanh, T., Unrath, A., Lahiri, N., Read, J., Say, M.J., Tabrizi, S.J., Kassubek, J., Kloppel, S., 2011. Stability of white matter changes related to huntington's disease in the presence of imaging noise: a dti study. PLoS currents 3, RRN1232.

Novak, M.J.U., Seunarine, K.K., Gibbard, C.R., Hobbs, N.Z., Scahill, R.I., Clark, C.A., Tabrizi, S.J., 2014. White matter integrity in premanifest and early huntington's disease is related to caudate loss and disease progression. Cortex 52, 98–112.

Oishi, K., Faria, A., Jiang, H., Li, X., Akhter, K., Zhang, J., Hsu, J.T., Miller, M.I., van Zijl, P.C.M., Albert, M., Lyketsos, C.G., Woods, R., Toga, A.W., Pike, G.B., Rosa-Neto, P., Evans, A., Mazziotta, J., Mori, S., 2009. Atlas-based whole brain white matter analysis using large deformation diffeomorphic metric mapping: application to normal elderly and alzheimer's disease participants. NeuroImage 46 (2), 486–499.

Orth, M., Gregory, S., Scahill, R.I., Mayer, I.SM., Minkova, L., Klöppel, S., Seunarine, K. K., Boyd, L., Borowsky, B., Reilmann, R., Bernhard Landwehrmeyer, G., Leavitt, B.R., Roos, R.AC., Durr, A., Rees, G., Rothwell, J.C., Langbehn, D., Tabrizi, S.J., 2016. Natural variation in sensory-motor white matter organization influences manifestations of huntington's disease. Hum. Brain Mapping 37 (12), 4615–4628.

Paulsen, J.S., et al., 2006. Preparing for preventive clinical trials: the predict-hd study. Arch. Neurology 63, 883–890.

Paulsen, J.S., et al., 2006. Brain structure in preclinical huntington's disease. Biolog. Psych. 59, 57–63.

Paulsen, J.S., et al., 2014. Prediction of manifest huntington's disease with clinical and imaging measures: a prospective observational study. Lancet Neurol. 13, 1193–1201.

Pecho-Vrieseling, E., et al., 2014. Transneuronal propagation of mutant huntingtin contributes to non–cell autonomous pathology in neurons. Nat. neuroscience 17, 1064–1072.

Pérot, J.-B., et al., 2022. Longitudinal multimodal mri characterization of a knock-in mouse model of huntington's disease reveals early grey and white matter alterations. Hum. Mol. Genet.

Pfefferbaum, A., Adalsteinsson, E., Rohlfing, T., Sullivan, E.V., 2010. Diffusion tensor imaging of deep gray matter brain structures: effects of age and iron concentration. Neurobiol. Aging 31, 482–493.

Phillips, O., Squitieri, F., Sanchez-Castaneda, C., Elifani, F., Griguoli, A., Maglione, V., Caltagirone, C., Sabatini, U., Di Paola, M., 2015. The corticospinal tract in huntington's disease. Cerebral Cortex 25 (9), 2670–2682.

Pierpaoli, C., Basser, P.J., 1996. Toward a quantitative assessment of diffusion anisotropy. Magn. Reson. Med. 36 (6), 893–906.

Poudel, G.R., et al., 2015. Longitudinal change in white matter microstructure in huntington's disease: The image-hd study. Neurobiol. disease 74, 406–412.

Poudel, G.R., Harding, I.H., Egan, G.F., Georgiou-Karistianis, N., 2019. Network spread determines severity of degeneration and disconnection in huntington's disease. Hum. Brain Mapping 40 (14), 4192–4201.

Reading, S.A.J., Yassa, M.A., Bakker, A., Dziorny, A.C., Gourley, L.M., Yallapragada, V., Rosenblatt, A., Margolis, R.L., Aylward, E.H., Brandt, J., Mori, S., van Zijl, P., Bassett, S.S., Ross, C.A., 2005. Regional white matter change in pre-symptomatic huntington's disease: a diffusion tensor imaging study. Psychiatry Res.: Neuroimaging 140 (1), 55–62.

Rezende, T.J., et al., 2019. Test–retest reproducibility of a multi-atlas automated segmentation tool on multimodality brain mri. Brain Behavior: Cognitive Neurosci. Perspective 9, e01363.

Rosas, H.D., et al., 2006. Diffusion tensor imaging in presymptomatic and early huntington's disease: Selective white matter pathology and its relationship to clinical measures. Mov. Disorders: Official J. Mov. Disord. Soc. 21, 1317–1325.

Rosas, H.D., Liu, A.K., Hersch, S., Glessner, M., Ferrante, R.J., Salat, D.H., van der Kouwe, A., Jenkins, B.G., Dale, A.M., Fischl, B., 2002. Regional and progressive thinning of the cortical ribbon in huntington's disease. Neurology 58 (5), 695–701.

Ross, C.A., et al., 2014. Huntington disease: natural history, biomarkers and prospects for therapeutics. Nature Rev. Neurol. 10, 204–216.

Ross, C.A., Reilmann, R., Cardoso, F., McCusker, E.A., Testa, C.M., Stout, J.C., Leavitt, B. R., Pei, Z., Landwehrmeyer, B., Martinez, A., Levey, J., Srajer, T., Bang, J., Tabrizi, S. J., 2019. Movement disorder society task force viewpoint: Huntington's disease diagnostic categories. Mov. Disorders Clinical Practice 6 (7), 541–546.

Rüb, U., et al., 2016. H untington's disease (hd): The neuropathology of a multisystem neurodegenerative disorder of the human brain. Brain Pathol. 26, 726–740.

Rüb, U., Hentschel, M., Stratmann, K., Brunt, E., Heinsen, H., Seidel, K., Bouzrou, M., Auburger, G., Paulson, H., Vonsattel, J.-P., Lange, H., Korf, H.-W., den Dunnen, W., 2014. H untington's d isease (hd): Degeneration of select nuclei, widespread occurrence of neuronal nuclear and axonal inclusions in the brainstem. Brain Pathol. 24 (3), 247–260.

Rubinsztein, D.C., et al., 1996. Phenotypic characterization of individuals with 30–40 cag repeats in the huntington disease (hd) gene reveals hd cases with 36 repeats and apparently normal elderly individuals with 36–39 repeats. Am. J. Human Gen. 59, 16.

Salat, D., et al., 2005. Age-related alterations in white matter microstructure measured by diffusion tensor imaging. Neurobiol. Aging 26, 1215–1227.

Saudou, F., Humbert, S., 2016. The biology of huntingtin. Neuron 89 (5), 910–926.

Scahill, R.I., et al., 2020. Biological and clinical characteristics of gene carriers far from predicted onset in the huntington's disease young adult study (hd-yas): a cross-sectional analysis. Lancet Neurol. 19, 502–512.

Sexton, C.E., et al., 2014. Accelerated changes in white matter microstructure during aging: a longitudinal diffusion tensor imaging study. J. Neurosci. 34, 15425–15436.

Snook, L., Plewes, C., Beaulieu, C., 2007. Voxel based versus region of interest analysis in diffusion tensor imaging of neurodevelopment. NeuroImage 34 (1), 243–252.

Steventon, J.J., Trueman, R.C., Rosser, A.E., Jones, D.K., 2016. Robust mr-based approaches to quantifying white matter structure and structure/function alterations in huntington's disease. J. Neuroscience Methods 265, 2–12.

Stoffers, D., Sheldon, S., Kuperman, J.M., Goldstein, J., Corey-Bloom, J., Aron, A.R., 2010. Contrasting gray and white matter changes in preclinical huntington disease: an mri study. Neurology 74 (15), 1208–1216.

Tabrizi, S.J., et al., 2013. Predictors of phenotypic progression and disease onset in premanifest and early- stage huntington's disease in the track-hd study: analysis of 36-month observational data. Lancet Neurol. 12, 637–649.

Tabrizi, S.J., Flower, M.D., Ross, C.A., Wild, E.J., 2020. Huntington disease: new insights into molecular pathogenesis and therapeutic opportunities. Nature Rev. Neurol. 16, 529–546.

Takahashi, M., et al., 2002. Magnetic resonance microimaging of intraaxonal water diffusion in live excised lamprey spinal cord. Proc. Nat. Acad. Sci. 99, 16192–16196.

Tan, B. *et al.* Longitudinal mapping of white matter tractography changes in huntington's disease: The image-hd study. (2022).

Tang, X., Oishi, K., Faria, A.V., Hillis, A.E., Albert, M.S., Mori, S., Miller, M.I., Rapallo, F., 2013. Bayesian parameter estimation and segmentation in the multi-atlas random orbit model. PLoS One1 8 (6), e65591.

Tang, X., Mori, S., Miller, M.I., 2014. Automated segmentation of corticospinal tract in diffusion tensor images via multi-modality multi-atlas fusion. In: Medical Imaging 2014: Biomedical Applications in Molecular, Structural, and Functional Imaging, vol. 9038. International Society for Optics and Photonics, p. 90381S.

van de Zande, N., Ghariq, E., de Bresser, J. & de Bot, S. Neuroimaging biomarkers for huntington's disease. (2022).

van der Plas, E. *et al.* Abnormal brain development in child and adolescent carriers of mutant huntingtin. *Neurology* **93**, e1021–e1030 (2019).

van der Plas, E., Schultz, J.L., Nopoulos, P.C., 2020. The neurodevelopmental hypothesis of huntington's disease. J. Huntington's disease 9 (3), 217–229.

Vaswani, A., et al., 2017. Attention is all you need. Adv. neural information processing systems 30.

Virlogeux, A., Moutaux, E., Christaller, W., Genoux, A., Bruyère, J., Fino, E., Charlot, B., Cazorla, M., Saudou, F., 2018. Reconstituting corticostriatal network on-a-chip reveals the contribution of the presynaptic compartment to huntington's disease. Cell Reports 22 (1), 110–122.

Vonsattel, J.-P., et al., 1985. Neuropathological classification of huntington's disease. J. Neuropathol. Exp. Neurol. 44, 559–577.

Waldvogel, H., Kim, E., Tippett, L., Vonsattel, J., Faull, R., 2015. The neuropathology of huntington's disease. Current Top. Behav. Neurosci. 22, 33–80.

Westlye, L.T., Walhovd, K.B., Dale, A.M., Bjornerud, A., Due-Tonnessen, P., Engvig, A., Grydeland, H., Tamnes, C.K., Ostby, Y., Fjell, A.M., 2010. Life-span changes of the human brain white matter: diffusion tensor imaging (dti) and volumetry. Cerebral Cortex 20 (9), 2055–2068.

Wijeratne, P.A., Garbarino, S., Gregory, S., Johnson, E.B., Scahill, R.I., Paulsen, J.S., Tabrizi, S.J., Lorenzi, M., Alexander, D.C., 2021. Revealing the timeline of structural mri changes in premanifest to manifest huntington disease. Neurol. Genet. 7 (5), e617.

Winklewski, P.J., Sabisz, A., Naumczyk, P., Jodzio, K., Szurowska, E., Szarmach, A., 2018. Understanding the physiopathology behind axial and radial diffusivity changes—what do we know? Front. Neurol. 9.

Wu, D., Ma, T., Ceritoglu, C., Li, Y., Chotiyanonta, J., Hou, Z., Hsu, J., Xu, X., Brown, T., Miller, M.I., Mori, S., 2016. Resource atlases for multi-atlas brain segmentations with multiple ontology levels based on t1-weighted mri. NeuroImage 125, 120–130.

Wu, D., Faria, A.V., Younes, L., Mori, S., Brown, T., Johnson, H., Paulsen, J.S., Ross, C.A., Miller, M.I., 2017. Mapping the order and pattern of brain structural mri changes using change-point analysis in premanifest huntington's disease. Hum. Brain Mapping 38 (10), 5035–5050.

Zeun, P. *et al.* Timing of selective basal ganglia white matter loss in huntington's disease. *bioRxiv* (2021).

Zhang, Y., et al., 2011. Indexing disease progression at study entry with individuals at-risk for huntington disease. Am. J. Med. Genet. Part B: Neuropsychiatr. Genet. 156, 751–763.

Zhang, J., Gregory, S., Scahill, R.I., Durr, A., Thomas, D.L., Lehericy, S., Rees, G., Tabrizi, S.J., Zhang, H., 2018. In vivo characterization of white matter pathology in premanifest huntington's disease. Ann. Neurol. 84 (4), 497–504.